Controlling the Electronic Structure of Bilayer Graphene

Taisuke Ohta,[1,2] *Aaron Bostwick,[1] * Thomas Seyller,[3] Karsten Horn,[2]

Eli Rotenberg[1**]

[1] Advanced Light Source, E. O. Lawrence Berkeley National Laboratory, USA

[2] Department of Molecular Physics, Fritz Haber Institute, Germany

[3] Institut für Physik der Kondensierten Materie, Universität Erlangen-Nürnberg, Germany

* Contributed equally to this work

** To whom correspondence should be addressed

We describe the synthesis of bilayer graphene thin films deposited on insulating silicon carbide and report the characterization of their electronic band structure using angle-resolved photoemission. By selectively adjusting the carrier concentration in each layer, changes in the Coulomb potential lead to a control of the gap between valence and conduction bands. This control over the band structure suggests potential application of bilayer graphene to switching functions in atomic-scale electronic devices.

Carbon-based materials such as carbon nanotubes (CNTs), graphite intercalation compounds (GICs), fullerenes, and ultrathin graphite films exhibit many exotic phenomena such as superconductivity (1,2,3) and anomalous quantum Hall effect (4,5,6). These findings have caused a renewed interest in the electronic structure of ultrathin layers of graphite, such as graphene, a single hexagonal carbon layer which is the building block for these materials. There is a strong motivation to incorporate graphene multilayers into atomic-scale devices, spurred on by rapid progress in their fabrication and manipulation.

We study the valence band structure of a bilayer of graphene, and demonstrate that through selective control of carrier concentration in the graphene layers, one can easily tune the band structure near the Dirac crossing. Similar control can be achieved in

principle by varying the electric field across the bilayer film in an atomic-scale switching device.

The electronic states of graphene can be well-described within basic calculational schemes (7,8,9). Graphene is a flat layer of carbon atoms arranged in a hexagonal lattice with two carbon atoms per unit cell. Of the four valence states, three sp^2 orbitals form a σ state with three neighboring carbon atoms, while one p orbital develops into delocalized π and π^* states which form the highest occupied valence band (VB) and the lowest unoccupied conduction band (CB). The π and π^* states of graphene are degenerate at the corner (K point) of the hexagonal Brillouin zone (BZ) (Fig. 1A). This degeneracy occurs at the so-called Dirac crossing energy E_D, which at the normal half-filling condition coincides with the Fermi level (E_F) resulting in a point-like metallic Fermi surface (see Fig. 2E).

Strictly speaking, undoped graphene is a semimetal because although there is a state crossing at E_D=E_F, the density of states there is zero and conduction is only possible with thermally excited electrons at finite temperature. In applying an effective mass description for the valence and conduction bands, (7) one arrives at a formal equivalence between the resulting differential equation and the Dirac equation, hence charge carriers in the vicinity of the Fermi level E_F may be termed "Dirac Fermions" (with the crossing point at K being named the "Dirac point"). Moreover, the particular band structure at the Brillouin zone boundary, i.e. a linear dispersion, leads to an effective mass $m^* = 0$ at the point where valence and conduction bands meet. The peculiar band structure in ultrathin

graphite layers results in a number of unusual electronic transport properties, such as an anomalous quantum Hall effect (4,5,6,10).

The graphene band structure is sensitive to the lattice symmetry. If the hexagonal layer structure is composed of non-equivalent elements, such as in boron nitride, the lateral, in-plane symmetry is broken, resulting in formation of a large gap between π and π^* states (11). The symmetry can also be broken with respect to the *c*-axis by stacking two graphene layers in Bernal stacking (the stacking fashion of graphite) as suggested by McCann and Fal'ko (12) (Fig. 1B). Since the unit cell of a bilayer contains four atoms, its band structure acquires two additional bands, π and π^* states, in each valley split by interlayer (A-B) coupling, and two lower-energy bands. If the individual graphene layers in a bilayer are rendered inequivalent (Fig. 1C), then, an energy gap between low-energy bands forms at the former Dirac crossing point (12). Provided that the charge state is such that the Fermi level lies within the gap, a semimetal-to-insulator transition occurs. If this symmetry breaking could be controlled externally, the electronic conductivity would change through this transition, suggesting that a switch with a thickness of two atomic layers could be constructed.

To see if this *gedanken* experiment can be realized, we have synthesized bilayer graphene films on a silicon carbide substrate (6H polytype with (0001) orientation), following the recipe in ref 13, and have measured their electronic properties using angle resolved photoemission spectroscopy (ARPES) 14. As initially grown, our films have a slight *n*-type doping, acquired by depletion of the substrate's dopant carriers. Because we measure at low temperature, the dopant electrons in the silicon carbide are frozen out

and the substrate is a nearly perfect insulator, while the excess carriers left in the film, having been separated from their dopant atoms, have a high mobility. As the SiC states are well-separated from both E_F and E_D (the SiC valence band lies ~2.6 eV below E_F, and the conduction band ~0.4 eV above E_F (15)), we can regard the bilayer graphene states as practically decoupled from the substrate and therefore as representing a true two-dimensional semi-metal.

These films can sustain high current densities. At 30K temperature, cold enough to preclude any conduction through the substrate, we can pass 400 mA through a macroscopic sample (5 × 15 mm), corresponding to a current of ~1 nA (10^{10}~10^{11} electrons per second) per graphene C atom, the same order of magnitude reported for single wall CNTs (16) and graphene multilayers (10).

The symmetry of the bilayers is broken by the dipole field created between the depletion layer of the SiC and the accumulation of charge on the graphene layer next to the interface, rendering the two graphene layers inequivalent with respect to charge and electrostatic potential in the as-prepared films. We can induce a further *n*-type doping by deposition of potassium atoms onto the vacuum side, which donate their lone valence electrons to the surface layer, forming another dipole (17,18). These surface and interface dipole fields together act as the symmetry-breaking factor which controls the presence or absence of the gap at the crossing energy E_D (Figs. 1B-C). The net dipole field between the two graphene layers results from the short screening length (~4 Å) along the *c*-axis (7) which is comparable to the layer thickness (~3.4 Å). A similar

charge localization has been observed at the surface of graphite and graphene multilayers in an externally applied field. (19,20)

Figs. 2A-C show the binding energy-momentum dispersion relation of π, π* and σ states along high symmetry directions measured by ARPES. The ~0.4 eV splitting of each of the π and π* states (as in Figure 1B) confirms that the sample is composed predominantly of two graphene layers (14). In Figs. 2A and B, the crossing point E_D can be clearly observed since this bilayer is doped *n*-type through carrier depletion from the SiC substrate. In the constant-energy contours in momentum space of π and π* states near E_F (Figs. 2D-F), we can clearly see the electron and hole pockets above and below E_D, respectively. Besides the primary bilayer graphene states, we can identify six weak replicas of the π and π* states surrounding the primary states, especially in Fig. 2F. Low energy electron diffraction shows that graphene layers grown on SiC substrate display a nearly commensurate superstructure with relative lattice constant ($6\sqrt{3} \times 6\sqrt{3}$) rotated 30° with respect to the substrate due to the difference between the graphene lattice constant of ~2.46Å and that of SiC, 3.07Å (21). The replicas of π and π* states are presumably brought about by scattering off of this superstructure in a similar fashion to other nearly incommensurate systems. (22,23)

The effects of doping the bilayers are shown in Fig. 3, which compares the as-prepared film (Fig. 3A) to two coverages of potassium. Our samples consist predominantly of bilayer graphene, but depending on preparation conditions, we find minority regions of single or triple layer graphene within our probe area; the contribution of these minority domains has been subtracted from the data in Fig. 3. Beside the more or less rigid shift of

the π and π* states toward higher binding energy due to an increased carrier concentration, the upper unoccupied π* state drops below E_F at n=0.0125 electron/unit cell (Fig. 3B) and continues dropping down with higher potassium coverage. The electron carrier densities of each stage are determined from the relative size of the Fermi surfaces with respect to the surface Brillouin zone of graphite.

Plotted next to the intensity maps are calculated tight-binding bands (solid lines) (12) where the low-lying electronic states near the K point of the Brillouin zone are described by the solution of a simple 4×4 Hamiltonian as:

$$\varepsilon_\alpha(k) = \pm\left[\frac{\gamma_1^2}{2} + \frac{U^2}{4} + \left(v^2 + \frac{v^3}{4}\right)k^2 + (-1)^\alpha\sqrt{\Gamma}\right]^{1/2}$$

where the band index α=1,2 and

$$\Gamma = \frac{1}{4}\left(\gamma_1^2 - v_3^2k^2\right)^2 + v^2k^3\left(\gamma_1^2 + U^2 + v_3^2k^2\right) + 2\gamma_1 v_3 v^2 k^3\cos 3\phi$$

and $v_3 = \sqrt{3}\,a\gamma_3/2\hbar$.

Here k is the momentum in Å^{-1}, ϕ is the azimuthal angle, v is the band velocity [m/s × $\hbar$ × 10^{10}], U is the difference in the on-site Coulomb potentials of the two layers, and γ_1 [eV] and γ_3 [eV] are out-of-plane nearest neighbor and next near neighbor interaction parameters (24,25). These parameters are adjusted to reproduce the measured band structures over a large energy range (14). U is chosen to match the gap at the K point.

The most important feature in Fig. 3 is the variation in the apparent gap at the K point - first open in Fig. 3A, then closed in Fig. 3B, and finally opened again in Fig. 3C. This

gap variation is reproduced by our tight-binding calculation and is attributed to the variation in the relative potentials of the two layers as discussed above. Away from the K point the gap is generally smaller than the prediction because the cusps extending into the gap between the π and π* bands are much sharper than in the model. As a result, the gap for the uncovered film (Fig. 3A) is not clearly resolved although a shift of the bands is readily apparent from the flattening of the π* band edge and the lack of spectral weight at E_D. Sufficient asymmetry was developed for higher doping that the gap is unambiguously opened in Fig. 3C.

It is also worth noting that the measured π* state of bilayer graphene (Fig. 3C) does not agree with the tight binding band particularly around 200 meV below E_F, where a slight kink is observed in the bands. This is presumably due to electron mass renormalization by electron-phonon coupling which will be discussed elsewhere (26).

In order to systematically follow the evolution of the gap between π and π* states, photoemission spectra at the K point (the center cut of the bands in Fig. 3) as a function of doping is shown in Fig. 4A. The blue markers are the positions of the tight-binding π and π* bands. The data and calculated energies of π and π* states clearly display the closing and re-opening of the gap. The yellow line is the energy difference E_F-E_D, which increases by about 0.32 eV with respect to the as-grown sample, reflecting the overall doping level of the film.

The variation of carrier concentration has a marked influence on the band structure as derived from a comparison of the experimental results with the tight-binding calculation (Fig. 4). The Coulomb potential difference U displays a sign change at the electron

concentration where the gap closes. It is expected that *U* increases with an increase of the charge difference in either graphene layer induced by the fields at the respective interfaces. We have calculated the potential of each graphene layer from Poisson's equation based on the Schottky barrier height of 0.4 eV (15) assuming infinitely thick graphene multilayers, and find that for the as-prepared sample the potential difference between the first and second layers shows reasonable agreement with the Coulomb potential difference *U* estimated from the size of the gap evaluated in the tight binding model. The resulting electric field in the graphene layers is similar in magnitude to that induced in a device structure (27). Moreover, a monotonic increase is seen in γ_1, which measures the interlayer interaction as a function of electron concentration in both layers. This suggests that at higher electron density, the overlap between π orbitals of adjacent graphene layers increases. This may be due to the smaller interlayer distance caused by a shorter screening length.

Our results demonstrate that by controlling the carrier density in a bilayer of graphene, the occupation of electronic states near the Fermi level, and the magnitude of the gap between valence and conduction bands can be manipulated. We have chosen potassium doping as a means of achieving this, but the switching functionality may be readily induced by an electric field across the bilayer in a device structure such that the potentials on either layer have opposite sign (10). The deposition of alkali atoms on epitaxially grown multilayer graphene films thus provides, beyond an opportunity to obtain their wave-vector-resolved electronic structure as reported here, a path to studying their physical properties in a device-like context.

1 Z. K. Tang *et al.*, Science 292, 2462 (2001).

2 N. B. Hannay *et al.*, Phys. Rev. Lett. **14**, 225 (1965).

3 T. E. Weller, M. Ellerby, S. S. Saxena, R. P. Smith, N. T. Skipper, Nature Physics **1**, 39 (2005).

4 K. S. Novoselov *et al*., Nature **438**, 197 (2005).

5 Y. Zhang, Y.-W. Tan, H. L. Stormer, P. Kim, Nature **438**, 201 (2005).

6 K. S. Novoselov *et al*., Nature Physics **2**, 177 (2006).

7 D. P. DiVincenzo, E. J. Mele, Phys. Rev. B **29**, 1685 (1984).

8 P. R. Wallace, Phys. Rev. **71**, 622 (1947).

9 S. Reich, J. Maultzsch, C. Thomsen, P. Ordejón, Phys. Rev. B **66**, 035412 (2002).

10 K. S. Novoselov *et al.*, Science **306**, 666 (2004).

11 X. Blase, A. Rubio, S. G. Louie, and M. L. Cohen, Phys. Rev. B **51**, 6868 (1995).

12 E. McCann, V. I. Fal'ko, Phys. Rev. Lett. **96**, 086805 (2006).

13 I. Forbeaux, J.-M. Themlin, and J.-M. Debever, Phys. Rev. B 58, 16396 (1998).

14 Information on materials and methods is available on Science Online.

15 Th. Seyller, K.V. Emtsev, F. Speck, K.-Y. Gao, L. Ley, Appl. Phys. Lett. in print.

16 Z. Yao, C. L. Kane, C. Dekker, Phys. Rev. Lett. **84**, 2941 (2000).

17 At 30K, the mobility of the potassium atoms is significantly reduced compared to at 90K where condensed phase of potassium atoms is found (see ref (18)). It is thus reasonable to assume that the potassium atoms mainly adsorb onto, and interact with the surface of the graphene layer in the low temperature deposition employed here (around 30K).

18 K. M. Hock and R. E. Palmer, Surf. Sci. **284**, 349 (1993).

19 Y. Zhang, J. P. Small, W. V. Pontius, and P. Kim, Appl. Phys. Lett. **86**, 073104 (2005).

20 K. S. Novoselov, F. Schedin, D. Jiang, A. A. Firsov, A. K. Geim, Phys. Rev. B **72**, 201401 (2005).

21 I. Forbeaux, J.-M. Themlin, J.-M. Debever, Phys. Rev. B **58**, 16396 (1998).

22 J. N. Crain, K. N. Altmann, C. Bromberger, and F. J. Himpsel, Phys. Rev. B **66**, 205302 (2002).

23 Eli Rotenberg *et al.*, Phys. Rev. Lett. **91**, 246404 (2003).

24 J. C. Slonczewski and P. R. Weiss, Phys. Rev. **109**, 272 (1958).

25 J. W. McClure, Phys. Rev. **108**, 612 (1957).

26 T. Ohta, A. Bostwick, T. Seyller, K. Horn, E. Rotenberg, unpublished.

27 S. V. Morozov *et al.*, Phys. Rev. B **72**, 201401 (2005).

28 This work and the ALS were supported by the Department of Energy, Office of Basic Sciences. K. H. and T. O. were supported by the Max Planck Society, and European Science Foundation under the EUROCORES SONS program.

Fig. 1. Electronic structure of (**A**) single (**B**) symmetric double layer and (**C**) asymmetric double layer of graphene. The energy bands depend only on in-plane momentum because the electrons are restricted to motion in a two-dimensional plane. The Dirac crossing points are at energy E_D.

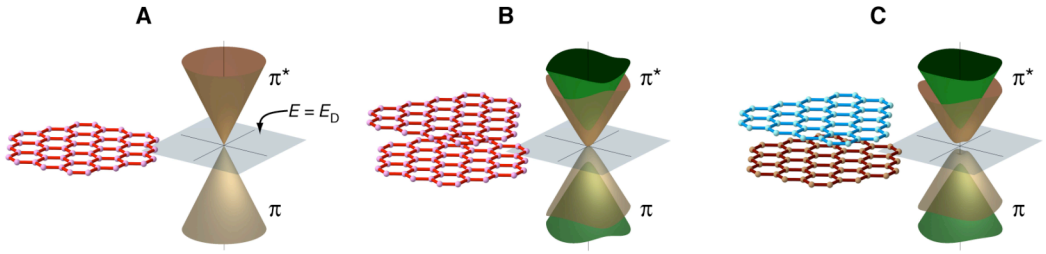

Fig. 2. Energy-momentum dispersion relation of π, π* and σ states of bilayer graphene. (**A-C**) energy-momentum dispersion along high symmetry directions. (**D-F**) constant energy contours at E_F, E_F - 0.4eV = E_D and - 2eV. The high symmetry points, directions, and Brillouin zone boundaries are indicated in (**D**).

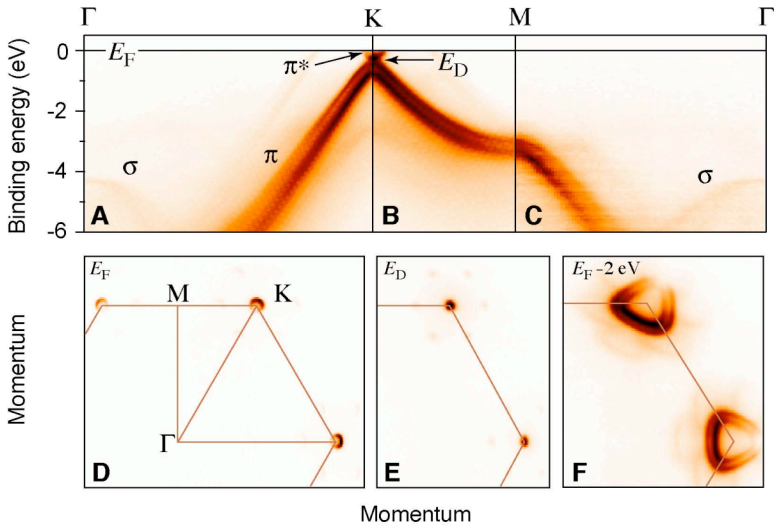

Fig. 3. Evolution of gap closing / reopening by changing the doping level by potassium adsorption. Experimental and theoretical bands (solid lines) for (**A**) as-prepared graphene bilayer and (**B-C**) with progressive adsorption of potassium. The number of doping electrons per unit cell, estimated from the relative size of Fermi surface, is indicated.

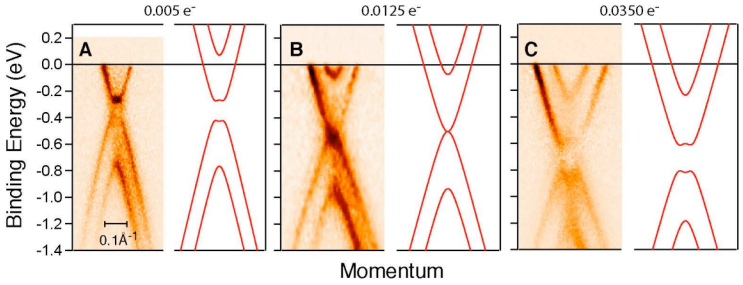

Fig. 4. Variation of states at the K point with increasing potassium coverage. (**A**) The image map shows the energy distribution curve at K as a function of potassium coverage. The blue markers are the fitted positions of the tight-binding π and π* bands, and the yellow line indicates E_D. The closing and re-opening of the gap between π and π* states are seen

clearly. (**B**) The influence of doping concentration on the band parameters U and γ_1.